

Relationship between Tropical Pacific SST and global atmospheric angular momentum in coupled models

Huei-Ping Huang¹, Matthew Newman², Richard Seager¹, Yochanan Kushnir¹
and Participating CMIP2+ Modeling Groups*

¹*Lamont–Doherty Earth Observatory of Columbia University, Palisades, New York*

²*NOAA–CIRES Climate Diagnostics Center, University of Colorado, Boulder, Colorado*

*CMIP2+ modeling groups are listed in Table 1.

January 2004

Corresponding address:
E-mail: huei@ldeo.columbia.edu
Phone : 845–365–8582
Fax : 845–365–8736

Abstract

The sensitivity parameter $S_1 = \Delta AAM / \Delta SST$, where ΔAAM and ΔSST represent the anomalies of global atmospheric angular momentum (AAM) and tropical Pacific sea surface temperature (SST) in the NINO3.4 region, is compared for the CMIP2+ coupled models. The parameter quantifies the strength of atmospheric zonal mean zonal wind response to SST anomaly in the equatorial Pacific, an important process for the climate system. Although the simulated ΔAAM and ΔSST are found to exhibit great disparity, their ratios agree better among the coupled models (and with observation) with no significant outliers. This indicates that the processes that connect the AAM anomaly to tropical SST anomaly are not sensitive to the base SST and the detail of convective heating and are relatively easy to reproduce by the coupled models. Through this robust ΔSST – ΔAAM relationship, the model bias in tropical Pacific SST manifests itself in the bias in atmospheric angular momentum. The value of S_1 for an atmospheric model forced by observed SST is close to that for a coupled model with a similar atmospheric component, suggesting that the ΔSST – ΔAAM relationship is dominated by a one–way influence of the former forcing the latter. The physical basis for the ΔSST – ΔAAM relationship is explored using a statistical equilibrium argument that links ΔSST to the anomaly of tropical tropospheric temperature. The resulting meridional gradient of tropospheric temperature is then linked to the change in zonal wind in the subtropical jets, the main contributor to ΔAAM , by thermal wind balance.

1. Introduction

Tropical Pacific sea surface temperature (SST) plays a key role in regulating global climate variability and change on intraseasonal to centennial time scales. The relationship between tropical Pacific SST and global climate can often be concisely represented by a simple sensitivity parameter, $S = \Delta CI / \Delta SST$, where CI is a global or large-scale climate index and ΔSST the SST anomaly averaged over a box in the tropical Pacific ocean. Figure 1a (adapted from Huang et al. 2003) illustrates such a relationship, using the observed monthly mean anomalies of global relative angular momentum (ΔAAM) and NINO3.4 index (as ΔSST). Here, the sensitivity parameter, $S_1 = \Delta AAM / \Delta SST$, is on the order of 1 angular momentum unit (AMU; $1 \text{ AMU} = 10^{25} \text{ kg m}^2 \text{ s}^{-1}$) per $^{\circ}\text{C}$ for a strong El Nino. Given the complicated structures in the SST and zonal wind (whose weighted global integral is AAM) or any other dynamical fields, simple climate indices illustrated by Fig. 1a are especially useful for the purpose of model intercomparison. This is recognized by previous researchers as the global ΔAAM has been used to compare the performances of atmospheric models in the Atmospheric Model Intercomparison Project (AMIP) (Hide et al. 1997), and those of coupled models in the Coupled Model Intercomparison Project (CMIP) (de Viron et al. 2002). At the same time, tropical SST (e.g., NINO3, NINO3.4) indices have also been widely used for model intercomparisons, including those performed for CMIP (AchutaRao and Sperber 2002). This study takes one step further to compare the relationship between the two climate indices. Thereby, the focus here is shifted from the variability in each of the two indices to the strength of the dynamical process that links them together. Specifically, the sensitivity parameter S_1 reflects the strength of atmospheric

zonal mean zonal wind response to a tropical SST anomaly in the NINO3.4 region. The increase of global atmospheric angular momentum in this case can be attributed to the acceleration of subtropical jets in *both* hemispheres as a canonical response to a positive tropical SST anomaly (see Kang and Lau (1994), Hoerling et al. (1995), Huang et al. (2003) and Seager et al. (2003) for useful surveys on the subject.) In a coupled model, the bias in the simulated ΔAAM could be due to a poorly simulated ΔSST or an unrealistic sensitivity in $S_1 = \Delta AAM/\Delta SST$, or both. Our work will help distinguish these possibilities.

Since a significant amount of power of tropical Pacific SST variability is concentrated in the seasonal to interannual frequency band, we will focus on this band to compare the aforementioned sensitivity parameter(s) in coupled models. It is worth noting that, even without coupling, some atmospheric general circulation models (AGCMs) forced by observed SST have been shown to produce an increase of global AAM during the warm phase of El Nino (e.g., Hide et al. 1997, Huang et al. 2003). An example, using the NCAR CCM3.10 (to be discussed in Sec. 3), is shown in Fig. 1b. Quantitatively, the sensitivity parameter S_1 has not been computed and compared among the AGCMs. This existing gap of knowledge notwithstanding, we will proceed to determine S_1 more precisely using coupled models that contain the feedbacks between ΔAAM and ΔSST . The difference between the sensitivity in AGCM and coupled GCM will be revisited in Sec. 3.

The ΔAAM – ΔSST relationship holds not only for climate variability, but also climate change induced by an increase of greenhouse gas (GHG) forcing. Huang et al. (2001) show that, in a set of coupled GCM (CCCma CGCM1) simulations with a transient increase of GHG concentration and sulphate aerosol loading, both global AAM and tropical

Pacific SST increases with time. As shown in Fig. 1c, the ratio of ΔAAM to $\Delta\text{SST}(\text{NINO}3.4)$ in this case remains roughly constant, leading to a well-defined sensitivity S_1 of about $0.75 \text{ AMU}/^\circ\text{C}$, comparable to that associated with El Nino. Räisänen (2003) shows that the value of a parameter similar to S_1 depends on the coupled models used for the global warming simulations. Our study is in the spirit of Huang et al. (2001) and Räisänen (2003), but focuses on the sensitivity parameter associated with the *internal* variability of the coupled system and on shorter (seasonal to interannual) time scales.

The AAM used in this paper is understood as the axial component of the angular momentum vector. The relationship between tropical SST and the equatorial components of angular momentum is not yet well-established and is not pursued. Our choice of global atmospheric angular momentum as an index for global climate is not arbitrary. Variations of global AAM have been shown to relate intimately to important phenomena of climate variability and change, ranging from Madden–Julian oscillation (Anderson and Rosen 1983, Madden 1987, Weickmann et al. 1997), El Nino (Rosen et al. 1984, Kang and Lau 1994), Quasi–biennial oscillation (Chao 1989), to global warming (Abarca del Rio 1999, Huang et al. 2001, de Viron et al. 2002, Räisänen 2003). On intraseasonal to interannual time scales, the anomaly of global AAM also has the attractive property of being approximately proportional to that of the length-of-day, which can be independently verified by geodetic measurements (e.g., Peixoto and Oort 1992). Other useful choices of global climate indices for coupled model intercomparisons will be discussed in Sec. 4.

2. Models and basic data

The total AAM is the sum of the relative angular momentum, M_R , that depends on the

strength and distribution of zonal mean zonal wind, and the "omega" angular momentum, M_Ω , that depends on the distribution of atmospheric mass (e.g., Peixoto and Oort, 1992). On seasonal to interannual time scales, the former dominates the variability in the total AAM (e.g., Huang et al. 2003). In the ensuing analysis, ΔAAM will be replaced by (and understood as) ΔM_R . The minor difference between the two is inconsequential to our discussion. The global relative angular momentum is defined by

$$M_R = R^3 g^{-1} \int_0^{p_s} \int_0^{2\pi} \int_{-\pi/2}^{\pi/2} u \cos^2 \phi d\phi d\lambda dp, \quad (1)$$

where R is the radius of the Earth, g the gravitational acceleration, u and p_s zonal velocity and surface pressure, and (ϕ, λ, p) latitude, longitude and pressure. The zonal wind (and, in some cases, surface pressure) fields required for the calculation are taken from the monthly mean archives of the CMIP2+ participating models. Because of monthly average, and because some of the wind data are archived on interpolated pressure levels (instead of the original terrain-following coordinates of the models), slight approximations are implied in the calculations of monthly M_R using Eq. (1). As detailed in Appendix A, these approximations produce only small errors that do not affect our discussion.

The CMIP2+ models are listed in Table 1. Details of these coupled models are available elsewhere (see the official web site of the CMIP project, <http://www-pcmdi.llnl.gov/cmip>). Unless otherwise noted, the control runs are used. The long-term mean and standard deviation of the monthly anomaly of AAM are listed in the 4th and 5th columns of Table 1. Before constructing the monthly anomaly, the time series are detrended with a 90-month high pass filter, which also helps to remove climate drift that

exists in some models. The standard deviation of the 9-month low-pass filtered (to be explained shortly) monthly anomaly of AAM is listed in the last column. Observed counterparts of these quantities, based on the NCEP–NCAR reanalysis (Kalnay et al. 1996) from 1979–1998, are listed at the bottom. While a longer record is available in the NCEP–NCAR reanalysis, the AAM derived from the zonal wind of the earlier period is not used as it is subject to a higher level of uncertainty and a "jump" in its value in the late 1970's (perhaps related to the so-called 1976/77 transition of climate regimes (Trenberth 1991)) that is not well-understood. These subtleties are discussed in Huang et al. (2003).

The long-term mean of global relative AAM simulated by the coupled models are roughly evenly distributed between 14.3 and 18.6 AMU, with the majority greater than the observed value (14.7). Only half of the models produce a long-term mean of AAM that does not depart from observation by more than 15 percent. (Previously, in the AMIP project, almost all forerunners of the atmospheric components of these coupled models satisfy the 15 percent criterion (Hide et al. 1997), when the AGCMs are forced by observed SST.) All but three of the coupled models simulated a standard deviation of the monthly anomaly of AAM (column 5 of Table 1) less than the observed value. When a 9-month low-pass filter is applied to the monthly anomaly (column 6), about 71 percent of the *variance* is retained for the observation. This ratio is below 60 percent (as low as 35 percent for the CSIRO model) for 6 of the 10 models, indicating too weak variability in the seasonal-to-interannual frequency band. A few models (notably MRI, HADCM3, and ECHO) do manage to produce a standard deviation of Δ AAM comparable to observation.

The standard deviations of monthly SST anomalies on the equator over the Pacific basin simulated by the CMIP2+ models are shown in Fig. 2. The characteristics of

the tropical Pacific SST produced by the CMIP2+ (our Fig. 2) and the slightly different CMIP2 (Fig. 1 of AchutaRao and Sperber 2002) models are very similar. More details about the interannual variability and annual mean of tropical Pacific SST in CMIP2 models can be found in AchutaRao and Sperber (2002) and are not repeated here. (The CMIP2+ dataset is chosen over CMIP2 because the former has a monthly resolution of atmospheric variables needed in our analysis. Note as well that the CMIP2 and CMIP2+ models are not identical. For example, the atmospheric component of the GFDL model analyzed by AchutaRao and Sperber (2002) has an R15 resolution, while its CMIP2+ counterpart R30.) The observation, based on the reconstructed Reynolds data set (Smith et al. 1996) from 1950–1999, is superimposed in Fig. 2. The observed standard deviation of monthly SST anomaly is uniformly high over the eastern and central Pacific, then drops sharply toward the western Pacific. Most of the coupled models do not reproduce this feature well. Nevertheless, most of them do produce substantial SST variability over the NINO3.4 region (marked by the red bar at bottom of Fig. 2), rendering the NINO3.4 SST index a useful choice as the denominator for defining the sensitivity parameter $S_1 = \Delta AAM / \Delta SST$. As a reminder, the NINO3.4 index is defined as the SST anomaly averaged over the box bounded by 5°N, 5°S, 170°W, and 120°W.

When viewed separately, the ΔAAM (Table 1) and ΔSST (Fig. 2) simulated by the coupled models exhibit great disparity. A careful inspection of them, however, reveals that the two models (CCCMA, CSIRO) with the lowest variance of ΔSST also have the lowest variance of ΔAAM . Likewise, the four models (ECHO, HADCM2, HADCM3, MRI) that produce the strongest seasonal-to-interannual variability of AAM also produce the

strongest variability of NINO3.4 SST anomaly. Thus, the ratio of the two climate indices, $\Delta\text{AAM}/\Delta\text{SST}$, may not depend on the models as strongly as do the individual indices. Recall that $S_1 = \Delta\text{AAM}/\Delta\text{SST}$ represents the strength of the physical process linking atmospheric zonal wind responses to tropical SST forcing, it is then possible that this process is consistently represented in the coupled models. Moreover, the robustness of the $\Delta\text{AAM}-\Delta\text{SST}$ relationship would imply that the model biases in the SST and AAM occur hand-in-hand. We should now examine S_1 for the CMIP2+ models.

3. Sensitivity parameters

Figure 3 shows the monthly anomalies of global relative angular momentum and NINO3.4 SST from an arbitrarily chosen 50-year segment for each CMIP2+ model. The time series are detrended with a 90-month high pass filter. While ΔAAM is clearly modulated by ΔSST at lower frequencies (seasonal to interannual time scales), at higher frequencies (sub-seasonal time scale) the former is noisier than the latter. (The AAM is known to have its own distinctive dynamics at the sub-seasonal time scales, e.g., that related to the intraseasonal oscillation (Weickmann et al. 1997)). Using observed daily data, Weickmann et al. (2001) estimated that the decorrelation time, t_d , for the internal variability of relative AAM is about one month. In other words, even without any SST anomaly, an AAM anomaly may exist for a particular month just by persistency from previous month. Thus, an average of the monthly data over a time span $t \gg t_d$ is needed to construct a meaningful sensitivity parameter S_1 . Guided by Weickmann et al. (2001), a 9-month low-pass filter is applied to both ΔAAM and ΔSST . The effect of the filter on

AAM is reflected in the difference between column 5 and 6 in Table 1, as already discussed. The 9-month filter has a relatively modest effect on the SST (not shown), as it has most of its power in the low frequency.

Figure 4 shows the scatter plots of the 9-month low-pass filtered ΔAAM and ΔSST from three models with their simulated variability of ΔAAM and ΔSST close to observation. Also shown are straight lines indicating the slope, i.e., $S_1 = \Delta AAM / \Delta SST$, determined from linear regression. (The intercepts obtained from the regression analysis are close to zero.) The slopes are all significantly positive, but differ quantitatively among the models. A slight asymmetry between warm ($\Delta SST > 0$) and cold events can be seen in Figs. 4a and 4b, with extreme warm events (e.g., $\Delta SST > 2.5$ C) outnumbering extreme cold events ($\Delta SST < -2.5$ C). These extreme events are relatively rare and do not significantly affect the slope in the regression analysis. To keep the intercomparison simple, we do not further separate the cold and warm events for the calculation of S_1 .

The S_1 for the CMIP2+ models are shown as open circles in Fig. 5, with the vertical sticks indicating twice the standard deviation of the slope obtained from the regression analysis. The observed value of S_1 , based on NCEP/NCAR reanalysis for 1979–1998, is indicated by the dashed line. The S_1 for the coupled models are comparable to, and roughly evenly distributed around, the observed value without significant outliers. The relatively large standard deviation of S_1 for the CCCMA and CSIRO models are expected, giving the small ΔAAM and ΔSST (therefore, a larger uncertainty in their ratio) they have. For these two models, even though their ΔSST and ΔAAM are outliers (with too weak seasonal-to-interannual variability), the ratio of the two falls within the range of the majority of the

models and the observation. This strengthens our argument that the process that links the atmospheric zonal wind response to tropical SST anomaly is consistently represented in the coupled models. Certainly, some differences still exist among the models (the scatter of the value of S_1 in Fig. 5 is comparable to its counterpart in the global warming case analyzed by Räisänen (2003)), as will be discussed in Sec. 4.

Since both ΔS_{ST} and ΔAAM are predicted in the coupled models, the strong relationship between them as shown above does not immediately imply causality. A comparison of S_1 for coupled and uncoupled models may shed some light on this issue. Sensitivity parameters such as S_1 have not been calculated for the AMIP or AMIP2 data, which, it should be noted, contain only a short run (10 and 17 yrs for AMIP and AMIP2, compared to 80–300 yrs for CMIP) for each model. Note as well that the atmospheric components of the CMIP2+ models are significantly revised versions that do not necessarily correspond closely to their AMIP/AMIP2 counterparts. Not attempting to re-analyze the AMIP/AMIP2 data, we will instead take a look at the difference in S_1 between coupled and uncoupled models using a 16-member ensemble of AGCM runs forced by observed SST. The model used is the NCAR CCM3.10 (with very slight modifications for execution on the computers at Lamont–Doherty Earth Observatory), an immediate forerunner of the atmospheric component of CSM and PCM. All runs are forced by identical SST from 1959–1999 but with different (randomly perturbed) initial conditions. Adopting the same treatment for observation, only the 1979–1998 segment is retained for our analysis. The sensitivity parameter S_1 is calculated for each run before ensemble averaging. The filled circle and accompanying vertical bar in Fig. 5 show the ensemble mean and intra-ensemble standard deviation of S_1 . Even without coupling, the S_1 for the AGCM is still significantly

positive, with its value close to (but slightly below) those for the coupled models (CSM and PCM) with a similar atmospheric component. One could infer that the strong relationship between ΔAAM and ΔSST in the coupled models and observation is dominated by the one-way influence of the SST forcing atmospheric zonal wind anomaly.

Since CSM produces a slightly higher value of S_1 than the uncoupled CCM3.10, one is tempted to declare that coupling increases the sensitivity. This speculation remains to be solidified when AGCM experiments for other CMIP2+ models return similar results. The AGCMs used would have to be identical, or as close as possible, to the atmospheric component of their corresponding coupled models. Practically, to improve the sampling for ΔSST (which is identical for our 16 AGCM runs), one could force the AGCMs with the SST time series produced by long coupled runs. Such experiments would form a very useful extension of the existing CMIP projects.

Our choice of the NINO3.4 index in defining S_1 has been an (otherwise useful) compromise, as the majority of the CMIP2+ models produce substantial SST variability over the central Pacific from 170°W to 120°W. However, since a few models have their variance of SST anomaly peaked in the far eastern or far western Pacific, it is useful to examine the dependence of S_1 on the choice of SST index. To do so, we replace the NINO3.4 index (as ΔSST) with a pan-Pacific index defined as the SST anomaly averaged over a box bounded by 5°N, 5°S, 150°E, and 90°W (the longitudinal extent of this box is the whole domain shown in Fig. 2). The S_1 re-calculated with this definition are shown in Fig. 6. As expected, their values increase from their counterparts in Fig. 5, since the SST anomaly averaged over the whole Pacific basin is generally weaker than that averaged over

the NINO3.4 region. Otherwise, the S_1 simulated by the coupled models remain comparable to that observed. Again, unlike the stand-alone ΔS_{ST} or ΔAAM , there are no significant outliers among the S_1 simulated by the CMIP2+ models.

4. Discussion

a. The AAM–SST relationship

The robustness of the ΔAAM – ΔS_{ST} relationship in the models and observation deserves further remarks. Since the tropically averaged SST and global AAM are proxies of tropical forcing and large-scale atmospheric circulation, to discuss their relationship one cannot avoid mentioning the two contrasting views (Emanuel et al. 1994) about the role of tropical convection in large-scale circulation. In the first, as stated in many textbooks, large-scale circulation is driven by tropical convective heating. An enhanced tropical convective activity would lead to a stronger Hadley circulation (e.g., Oort and Yienger 1996) accompanied by a stronger subtropical jet, thereby a higher value of global angular momentum. In this picture, tropical SST affects global AAM by changing the convective heating that directly forces the latter. In the alternate view, called "statistical-equilibrium thinking" (Emanuel et al. 1994, and references therein) tropical convection and the large-scale environment (temperature, moisture, etc.) are nearly in statistical equilibrium (since the former adjusts to changes in the latter on a very short time scale), that one does not drive another. In this view, convection acts to maintain the observed quasi-equilibrium state with an approximately moist virtual adiabatic profile extending up to the freezing level (Betts 1986). Based on this latter idealization, the thermodynamic structure of the troposphere in the convecting regions is controlled by the sub-cloud layer entropy, S_B

(Emanuel et al. 1994), which is closely related to SST (Emanuel et al. 1994, Lindzen and Nigam 1987). An enhanced meridional SST gradient would then lead to an increase in the meridional gradient of tropospheric temperature and, by thermal wind balance, a stronger subtropical jet in the upper troposphere.

Before proceeding further, it should be noted that most AMIP models (representative of the atmospheric components of CMIP models) forced by observed SST produce too weak interannual variability of tropical precipitation (an indicator of convective heating), with its amplitude one order of magnitude smaller than that observed (Soden 2000). If the tropical large-scale circulations (Hadley circulation, subtropical jets) in the models were directly controlled by convective heating one would expect poorly simulated values of $\Delta\text{AAM}/\Delta\text{SST}$. The fact that this is not the case indicates that tropical large-scale circulations in the AGCMs are not critically controlled by convective heating. At the same time, despite the problem in precipitation, Soden (2000) shows that the simulated interannual variability of tropical tropospheric temperature and moisture agree much better with observation. Regardless of the detail of convection, the correct temperature field would, by thermal wind balance, imply a correct zonal wind field and a realistic value of global angular momentum. These considerations favor an interpretation of our results based on the statistical equilibrium (SE) thinking, which we will explain further.

The useful point in the SE thinking is the relationship between (the meridional gradients of) tropospheric temperature and sub-cloud layer entropy (cf. pp. 1123, 1136 of Emanuel et al. 1994),

$$\frac{\partial \alpha}{\partial \phi} \approx \gamma \frac{\partial S_B}{\partial \phi} , \quad (2)$$

where α is the specific volume of the atmosphere, γ the reversibly–defined moist adiabatic (or "moist virtual adiabatic") lapse rate $(dT/dp)_{S, \text{moist virtual}}$, ϕ latitude, and the derivative in the left hand side performed at constant pressure. We next attempt to relate the right hand side of Eq. (2) to SST, and left hand side to AAM. The low level entropy S_B is constantly restored back to the surface entropy, S_{sfc} , by boundary layer mixing. Assuming that the mixing process is very efficient, one may, for the sake of argument, replace S_B with S_{sfc} ,

$$\frac{\partial S_B}{\partial \phi} \approx \frac{\partial S_{sfc}}{\partial \phi} , \quad (3)$$

but keep in mind that the latter is more likely the upper bound of the former over the tropical oceans. Using the definition, $dS = c_p d\ln\theta_e$ (c_p and θ_e are heat capacity at constant pressure and equivalent potential temperature), and replacing surface air temperature with SST over the ocean, one obtains

$$dS_{sfc} = c_p d\ln SST + Ld(w_s/SST) \quad (4a)$$

$$\approx (SST)^{-1}[c_p dSST + Ldw_s] \quad (4b)$$

$$= (SST)^{-1}[c_p dSST + LbdSST] \quad (4c)$$

$$= B (SST)^{-1}dSST \quad , \quad (5)$$

where w_s is the saturation mixing ratio at surface, L the latent heat constant over liquid water, and $B = c_p + Lb$ with

$$b = \frac{dw_s}{dSST} . \quad (6)$$

From (4a) to (4b) one uses the approximation $dw_s/w_s \gg dT/T$ (e.g., Wallace and Hobbs 1977, p.104), which is readily verified in Appendix B. While w_s is generally a nonlinear function of temperature, for the narrow range of SST (in the tropical and subtropics) of our

interest b is approximately a constant. A linear least square fit for the range $18^\circ\text{C} < \text{SST} < 32^\circ\text{C}$ gives $b = 1.17 \pm 0.06 \text{ g}(\text{kg})^{-1}(\text{K})^{-1}$ (Appendix B). Thus, one obtains

$$\frac{\partial S_B}{\partial \phi} \approx \frac{B}{\text{SST}} \frac{\partial \text{SST}}{\partial \phi} . \quad (7)$$

The left hand side of Eq. (2) can be linked to AAM through thermal wind balance (Räsänen 2003). Denoting the geostrophic component of zonal wind as u_G , a vertical integration of the thermal wind relationship (for simplicity, ignore curvature term and consider temperature instead of virtual temperature) combined with Eq. (2) and (7) yields

$$u_G(p) - u_G(p_s) = \frac{-1}{2R\Omega \sin \phi} \int_p^{p_s} \frac{\partial \alpha}{\partial \phi} d\hat{p} \quad (8)$$

$$\approx \frac{-B}{2R\Omega \sin \phi} h \frac{1}{\text{SST}} \frac{\partial \text{SST}}{\partial \phi} , \quad (9)$$

where

$$h = \int_p^{p_s} \gamma d\hat{p} .$$

When applying Eq. (9), we will avoid the vicinity of the equator where the smallness of the Coriolis parameter renders the expression singular. Equation (9) can be used to evaluate global angular momentum if one replaces the zonal wind, u , in Eq. (1) with $u_G(p) - u_G(p_s)$. In Räsänen's notation, this is to consider only the M_{RbG} component of the total relative angular momentum, M_{R} . (The subscripts b and G stand for baroclinic and geostrophic.) This involves two approximations, namely, (i) The total wind is replaced by its geostrophic component, u_G , and (ii) The contribution of the surface component $u_G(p_s)$ to (the variability of) global angular momentum is neglected. Räsänen (2003) shows that (i) is a good

approximation, while (ii) might cause a sizeable error depending on circumstances. With this caution in mind, using Eq. (1) and (9) one obtains,

$$\begin{aligned}
M_{RbG} &\approx -K \int_0^{p_s} \int_0^{2\pi} \int_{-\pi/2}^{\pi/2} \frac{\cos^2 \phi}{\sin \phi} h \frac{1}{SST} \frac{\partial SST}{\partial \phi} d\phi d\lambda dp \\
&\approx -K \int_0^{2\pi} \int_{-\pi/2}^{\pi/2} \frac{\cos^2 \phi}{\sin \phi} H \frac{\partial SST}{\partial \phi} d\phi d\lambda , \tag{10}
\end{aligned}$$

where $K = R^2 B(2\Omega g)^{-1}$, and

$$\begin{aligned}
H &= \frac{1}{SST} \int_0^{p_s} h dp \\
&\approx p_s \left(1 - \frac{\langle T \rangle}{SST}\right) ,
\end{aligned}$$

with $\langle T \rangle$ the vertically averaged temperature for the moist virtual adiabatic profile. To the extent that H does not vary significantly in the tropics (the total SST varies by about 1 percent, and $\langle T \rangle$ is determined by SST), the integral in (10) is determined mainly by the domain-averaged meridional gradient of SST. Again, it is understood that the integral will bypass the vicinity of the equator where the integrand becomes singular. (A numerical integration of Eq. (10) or the like is feasible if one replaces the value of the integrand at the equator with that of an average over the grid points closest to the equator (Räsänen 2003).) While the meridional integral in Eq. (10) is from pole to pole, statistical equilibrium (and other assumptions such as the constancy of B) holds only in the lower latitudes. This is perhaps not a major concern if one is interested in the effect of El Nino SST anomaly on the anomaly of M_{RbG} . In that case, the meridional gradient of ΔSST is confined to the lower latitudes and the integrand (when cast in its anomalous form) vanishes outside the tropics.

Likewise, in that problem, the integration in λ could be restricted to the longitudes where the anomaly of SST is large. With the SST change confined to the tropics, a change in the SST itself immediately implies a change in the meridional SST gradient. To that extent, the meridional gradient of ΔSST is proportional to the tropically averaged ΔSST by a geometric constant.

To summarize, Eq. (10) implies that *the change in the (baroclinic component of) angular momentum is controlled by the change in the domain-averaged meridional gradient of SST, which is in turn related to the tropically-averaged SST anomaly if the SST outside the tropics remains unchanged.* This provides the basis for the robust ΔAAM - ΔSST relationship in the models and observation. Moreover, although the total SST is embedded in H in Eq. (10), it does not significantly affect the value of the integration. This explains why the parameter $S_1 = \Delta\text{AAM}/\Delta\text{SST}$ is not sensitive to the base value of SST in the coupled models. That the integrand in Eq. (10) does not involve the east-west gradient of SST may also explain why the behavior of the S_1 parameter is not sensitive to the longitudinal location and extent of the box used for averaging ΔSST .

Due to the many approximations involved, Eq. (10) is more useful for a qualitative understanding of the ΔSST - ΔAAM relationship than for an accurate evaluation of the ratio $\Delta\text{AAM}/\Delta\text{SST}$ from the first principle, which remains a challenge. Our assumption that ΔS_B is determined by ΔSST may be meaningful in the context of the ΔSST - ΔAAM relationship associated with El Nino. In general, however, boundary layer mixing is affected by other factors, notably the surface wind speed. In fact, the dependence of S_B on surface wind speed is key to the evaporation-wind feedback theory for tropical cyclone (Emanuel et al. 1994)

(although the surface wind anomaly associated with a tropical cyclone is certainly much larger than that associated with El Niño). The contribution of the surface zonal wind anomaly to ΔAAM is also neglected in our derivation when ΔM_R is replaced by ΔM_{RbG} . How the effects of surface wind may quantitatively modify our conclusion remains to be investigated.

While borrowing Eq. (2) from the statistical equilibrium thinking to aid our discussion, we are aware that some of the GCMs apparently do not employ a cumulus parameterization scheme entirely consistent with SE. For example, the Arakawa–Schubert scheme is more consistent with SE, while the original Kuo scheme is related to the contrasting idea of CISK (conditional instability of the second kind) that allows a significant accumulation and release of CAPE (convective available potential energy) (Emanuel et al. 1994). These may be reconcilable for several reasons. First, the diabatic heating in a modern GCM is usually determined by a mixture of interconnected schemes for deep and shallow convection, large–scale condensation, and boundary layer. Even a Kuo–type scheme is connected to the parameterization of boundary layer and surface fluxes, the latter omitted in the original CISK theory. Thus, the behaviors of GCMs could have more in common than that suggested by the generic names (Kuo, Arakawa–Schubert, etc.) of their convective schemes. As a telling example, Wang and Schlesinger (1999) show that the behavior of the simulated Madden–Julian oscillation in a GCM employing a switchable (Kuo, Arakawa–Schubert, or moist convective adjustment) convective scheme is determined not by the type of the scheme, but by the value of a parameter, RH_c (the threshold of low–level relative humidity for convection to occur) that is common to all three schemes. On the other hand, the differences in the convective schemes may contribute to the differences in

the values of S_1 in Fig. 5 and 6. For example, the moist convective adjustment (MCA) scheme (Manabe et al. 1965) tends to restore the atmospheric profile to a moist adiabat (with condensed water precipitating immediately), while the Betts–Miller scheme (Betts 1986, Betts and Miller 1986) restores the vertical profile to a relatively cooler moist virtual adiabat (condensed water allowed to stay in the air parcel). Given the same ΔSST , one would expect the two schemes to produce somewhat different sensitivity in $\Delta T_A/\Delta\text{SST}$, where T_A is the tropospheric air temperature, and thereby different sensitivity in $\Delta\text{AAM}/\Delta\text{SST}$ by the argument of thermal wind balance.

b. El Nino and atmospheric angular momentum

Given that our argument of the ΔAAM – ΔSST relationship does not depend critically on the detail of convection and the base value of SST, one would expect an El Nino SST anomaly (which peaks at the equator with roughly the same $|\partial\Delta\text{SST}/\partial\phi|$ on both sides of it) to produce hemispherically symmetrical responses in subtropical zonal winds in both hemispheres that are insensitive to season. This is consistent with the analysis by Seager et al. (2003) for both observation and GCM simulations. Note that El Nino SST anomalies also cause interesting changes in the large–scale circulation in the higher latitudes (e.g., Seager et al. 2003), but these features are relatively unimportant for global angular momentum, due to the $\cos^2\phi$ weight in Eq. (1).

While our discussion bypasses the detail of convection by adopting the statistical equilibrium thinking, it does not rule out the possibility that the detailed distribution of tropical convective heating may, under some circumstances, be relevant to the responses in

the subtropical jets. To aid the discussion, consider the zonally symmetric models of Hadley circulation (Held and Hou 1980, Lindzen and Hou 1988). On the one hand, it is true that the classical Held–Hou model does not depend explicitly on the detail of diabatic heating; The extent of Hadley cell and the strength of subtropical jet are controlled by the imposed (with Newtonian relaxation) meridional temperature gradient. On the other hand, Lindzen and Hou (1988) shows that a small shift of the ascent off the equator could cause a much stronger Hadley circulation in the opposite hemisphere. Since the location of ascent is related to the location of intense convection, the detail of the latter becomes relevant. This aspect is not covered by our general discussion based on statistical equilibrium. There is evidence that, during the winter seasons of El Nino events, a positive precipitation anomaly appears south of the equator in the central Pacific at the longitude where the positive zonal wind anomaly in the N. H. subtropics has a maximum (Seager et al. 2004, submitted to J. Climate). However, even in this case, an approximately hemispherically symmetric pattern, including a positive anomaly in the S.H., of zonal wind anomaly still exist at this longitude, indicating that the simple statistical equilibrium argument still works. Thus, the very specific aspect of the southward shift of convection contributes mainly to the asymmetric part of the response, making the N. H. zonal wind anomaly stronger than its S. H. mirror image. We leave these interesting details to a separate paper (Seager et al. 2004, submitted).

c. Other sensitivity parameters

The S_1 analyzed in this study is just an example of the sensitivity parameters that quantify the strength of the physical process(es) linking two components of the climate

system. Previously, useful model intercomparisons have been performed within the AMIP (e.g., Gates et al. 1999) and CMIP (e.g., Lambert and Boer 2001) frameworks with more emphases on the climatology and basic statistics of individual fields (temperature, wind, etc.) but relatively less on the relationships between two fields. Understandably, an intercomparison of the latter type is more difficult, giving the potentially large degrees of freedom resulted from combining two fields together. Our study shows an example to simplify the problem by choosing a pair of large-scale climate indices as proxies of the 2-D or 3-D fields. That this choice is meaningful has been explained in Sec. 4a.

In light of our discussion in Sec. 4a and 4b, an analysis of the relationship between ΔSST and tropospheric temperature in the coupled models would be very useful. A positive tropical Pacific SST anomaly usually leads to warming in the tropical/subtropical troposphere (e.g., Yulaeva and Wallace 1994), and cooling in the midlatitude north of 40° (e.g., Seager et al. 2003). Using the anomaly of tropospheric temperature, ΔT_A , as the numerator, the sensitivity parameter $S_2 = \Delta T_A / \Delta\text{SST}$ would be a meaningful choice for further model intercomparisons. In addition, S_2 is useful for separating El Niño-induced tropospheric temperature variability from global warming signals in observation and coupled model simulations (Santer et al. 2001). As the maximum of tropically averaged ΔT_A is known to lag that of ΔSST by 1–2 seasons depending slightly on the choice of the box for averaging ΔSST (Angell 2000, Chiang and Sobel 2002, Sobel et al. 2002), S_2 would generally depend on the time lag with $S_2(\tau) = \Delta T_A(t+\tau) / \Delta\text{SST}(t)$. (This does not affect our analysis of the $\Delta\text{AAM}-\Delta\text{SST}$ relationship due to the 9-month low pass filter.)

In general, the relationship between a pair of large-scale climate indices can be

even more complicated than that represented by S_1 or S_2 . For example, one index may depend on the cumulative contribution of the other through the past history, such that the former is a time integrator of the latter. An interesting case of such a relationship is explored by Newman et al. (2003), in which the Pacific Decadal Oscillation (Zhang et al. 1997) index (ΔPDO) and the El Niño index (similar to our ΔSST) are related by $\Delta\text{PDO}(t) = \alpha \Delta\text{PDO}(t-\delta t) + \beta \Delta\text{SST}(t) + \eta(t)$, where δt is one year, $\eta(t)$ a stochastic component, and ΔPDO and ΔSST the annually averaged anomalies of the indices. The parameter α quantifies the year-to-year memory of ΔPDO (through the re-emergence mechanism, e.g., Alexander et al. 1999), and β the contribution of El Niño. Hindcasts of ΔPDO using the simple model have met remarkable success (Newman et al. 2003), indicating the potential of quantifying complicated atmosphere-ocean processes by a small numbers of climate indices. The $S_2(\tau)$ and (α, β) are but two examples of useful generalizations of S_1 that we plan to pursue for further model intercomparisons. Sensitivity parameters arising from the combinations of other global or large-scale climate indices (e.g., Karoly and Braganza 2001) are worth investigations.

5. Conclusions

The sensitivity parameter $S_1 = \Delta\text{AAM}/\Delta\text{SST}$ is compared for the CMIP2+ models. The parameter quantifies the strength of atmospheric zonal mean zonal wind response to SST anomaly in the NINO3.4 region in the equatorial Pacific. When viewed separately, the ΔAAM (anomaly of global atmospheric angular momentum) and ΔSST (NINO3.4 SST index) simulated by the coupled models exhibit great disparity. However, a small (large)

Δ SST is found to usually accompany a small (large) Δ AAM in these simulations, giving rise to a much higher degree of consistency in the ratio Δ AAM/ Δ SST among the models and the observation. This indicates that the processes that produce atmospheric zonal wind response to tropical SST anomaly are not too sensitive to the base value of SST and the detail of tropical convective heating and are relatively easy to reproduce by the coupled models. At the same time, through this robust Δ AAM– Δ SST relationship, the model bias in tropical pacific SST would tend to manifest itself in the bias in atmospheric angular momentum.

The robust Δ SST– Δ AAM relationship is explained based on a statistical equilibrium argument that links the tropical Δ SST to tropospheric temperature anomaly. During El Nino when Δ SST is concentrated in the tropics, the increase in tropical Pacific SST implies an increase in the meridional gradient of SST, which in our argument produces an increase in the meridional gradient of tropospheric temperature. By thermal wind balance, the latter corresponds to an increase of the vertical shear in the subtropics, or an enhancement of the subtropical jets if the surface wind is assumed unchanged. The enhanced subtropical jets implies a positive Δ AAM, completing the Δ SST– Δ AAM connection.

The value of S_1 for an AGCM forced by observed SST is close to, but slightly below, that for a coupled model (whose atmospheric component is modified from the AGCM), suggesting that the Δ SST– Δ AAM relationship is dominated by a one–way influence of the former forcing the latter. Although our limited results show a slightly enhanced sensitivity in S_1 with coupling, this conclusion remains to be solidified with more comparisons among pairs of coupled and uncoupled models.

Climate model intercomparisons based on the AMIP and CMIP data sets have produced fruitful results in the last decade. Most of previous AMIP/CMIP studies address the similarities and differences in a single field, instead of those in the relationship between two fields among the GCMs. Despite its apparent complexity, the latter type of analysis is shown to be feasible if the two fields can be meaningfully represented by a pair of climate indices. Our analysis of S_1 highlights the potential of such an approach, which we expect to be more widely adopted in future GCM intercomparison studies.

Acknowledgements

This paper constitutes the first part of the report for the CMIP2+ diagnostics subproject entitled "Relationship between tropical Pacific SST and large-scale climate indices in coupled models". The authors thank Curt Covey for help with the CMIP2+ data, Naomi Naik for advices on data processing, and Klaus Weickmann for discussions.

Appendix A: Approximations in the calculations of M_R

The global relative angular momentum is computed from the discretized version of Eq. (1),

$$M_R \approx R^3 g^{-1} \sum_{i=1}^{NX} \sum_{j=1}^{NY} \sum_{k=1}^{NZ} u(i,j,k) \cos \phi_j w_j \Delta \lambda (\Delta p)_{i,j,k} , \quad (\text{A1})$$

where (i, j, k) are the longitudinal, meridional, and vertical indices of the three dimensional fields, and ϕ_j and w_j the Gaussian latitudes and weights. For data archived on pressure coordinates (all models except GFDL, CSM, and PCM),

$$(\Delta p)_{i,j,k} = (\Delta p)_k , \quad (\text{A2})$$

where $(\Delta p)_k$ is independent of time. Calculations of monthly M_R from this type of data are straightforward, as they only require the use of monthly mean zonal wind. The interpolation of winds from the original terrain-following coordinates to pressure coordinates may result in small errors (around 2 percent for daily M_R , Madden and Speth 1995, Huang et al. 1999) that are otherwise tolerable for our purpose. (Note that the increase of M_R associated with a strong El Nino can be as much as 15–20 percent of its climatological value.)

For data available on a sigma coordinate (GFDL model),

$$(\Delta p)_{i,j,k} = p_s(i,j) (\Delta \sigma)_k , \quad (\text{A3})$$

where $p_s(i, j)$ is the time varying surface pressure field. In addition, the CSM and PCM model outputs are available on their original hybrid coordinates defined by

$$p(i,j,k) = A_k P_0 + B_k p_s(i,j) , \quad (\text{A4})$$

where A_k , B_k , and P_0 are constants but $p_s(i,j)$ varies with time (therefore the pressure levels, $p(i,j,k)$, also vary with time). The $(\Delta p)_{i,j,k}$ in (A1) is obtained from the difference of p at k and $k+1$. For the sigma- and hybrid-coordinate data, the calculations of monthly M_R in our analysis are precise in space but slightly compromised in time. Ideally, the monthly mean M_R is obtained by averaging daily M_R derived from daily u and p_s . Given that daily model archives are not available for most CMIP models, the monthly mean u and p_s are used in (A1) for the calculation of monthly M_R . To discuss the impact of this approximation, first note that (A1) is equivalent to a weighted summation of the product of u and p_s (since $(\Delta p)_{i,j,k}$ can be represented as $p_s(i,j)$ multiplied by some constant(s)). Symbolically, the

precise value of the monthly M_R (derived from daily u and p_s) can be decomposed as

$$\Sigma \langle u p_s \rangle = \Sigma \langle u \rangle \langle p_s \rangle + \Sigma \langle u' p_s' \rangle , \quad (\text{A5})$$

where Σ denotes the weighted 3-D summation, bracket the monthly average and primed quantities the departure from monthly mean. In our calculation only the first term in the right hand side is retained. This is justifiable, since $\langle p_s \rangle$ is on the order of 1000 hPa while p_s' rarely exceeds 20–30 hPa and only for localized disturbances (such as wintertime weather systems) that do not have a global correlation with u' . Moreover, the temporal correlation between p_s' and u' is likely small on the monthly time scale, since transient eddies with large p_s' usually come and go randomly on a weekly time scale. These considerations put the error in our approximation at about 1 percent of the total. To solidify this estimate, an experiment is performed by running an atmospheric model, the NCAR CCM3.10 (which has the same resolution and arrangement of the hybrid coordinate as the atmospheric component of CSM), for a month forced by observed SST. The u and p_s fields are saved every 6 hours, enough for an accurate evaluation of the monthly M_R . The precise monthly mean M_R for a model September is 15.548 AMU. Our approximation (first term in the r.h.s of (A5)) yields the value of 15.568 AMU, with the residue (second term in the r.h.s) being only 0.02 AMU. In sum, the monthly mean M_R evaluated from the monthly archives of the coupled models are only subject to small errors that do not affect the conclusions of this paper.

Appendix B: Dependence of w_s on SST in the tropics

At sea surface, the saturation mixing ratio is only a function of SST, with $w_s(\text{SST})$

$\approx 0.622 e_s(\text{SST})/p_s$, where e_s is saturation vapor pressure and $p_s \approx 1013.6$ hPa. In the tropics/subtropics between 30°N and 30°S , the values of SST fall within the range of 20 – 30°C . The exact values of w_s obtained from a standard formula of $e_s(T)$ (e.g., Gill 1982, Appendix 4), are shown in Fig. 7 as filled circles for $18^\circ\text{C} < \text{SST} < 32^\circ\text{C}$. Within this range, the relationship between dw_s and $d\text{SST}$ is approximately linear. A linear least square fit, shown as the dashed line, yields a slope of $b = 1.17 \pm 0.06 \text{ g}(\text{kg})^{-1}(\text{K})^{-1}$. Since a 1°K increase in SST corresponds to about 1 g/kg increase in saturation mixing ratio, one also verifies the approximation used in Eq. (4b) that $dw_s/w_s \gg d\text{SST}/\text{SST}$ (since from Fig. 7 the w_s in the denominator is about 20 g/kg for $\text{SST} \approx 300^\circ\text{K}$).

References

- Abarca del Rio R (1999) The influence of global warming in earth rotation speed, *Ann Geophys* 17: 806–811
- AchutaRao K, Sperber KR (2002) Simulation of the El Nino Southern Oscillation: results from the coupled model intercomparison project, *Clim Dyn* 19: 191–209.
- Alexander MA, Deser C, Timlin MS (1999) The re-emergence of SST anomalies in the North Pacific Ocean, *J Climate* 12: 2419–2431
- Anderson JR, Rosen RD (1983) The latitude–height structure of 40–50 day variations in atmospheric angular momentum, *J Atmos Sci* 40: 1584–1591
- Angell JK (2000) Tropospheric temperature variations adjusted for El Nino, 1958–1998, *J Geophys Res* 105: 11841–11849
- Betts AK (1986) A new convective adjustment scheme. Part I: observational and theoretical basis, *Q J R Meteorol Soc* 112: 677–691
- Betts AK, Miller MJ (1986) A new convective adjustment scheme. Part II: single column tests using GATE wave, BOMEX, ATEX, and arctic air–mass data sets, *Q J R Meteorol Soc* 112: 693–709
- Chao BF (1989) Length–of–day variations caused by El Nino–southern oscillation and quasi–biennial oscillation, *Science* 243: 923–925
- Chiang JCH, Sobel AH (2002) Tropical tropospheric temperature variations caused by ENSO and their influence on the remote tropical climate, *J Climate* 15: 2616–2631
- de Viron O, Dehant V, Goosse H, Crucifix M, Participating CMIP Modeling Groups (2002) Effect of global warming on the length–of–day, *Geophys Res Lett* 29: doi:10.1029/2001GL013672.

- Emanuel KA, Neelin JD, Bretherton CS (1994) On large-scale circulations in convecting atmospheres, *Q J R Meteorol Soc* 120: 1111–1143
- Gates WL, Boyle JS, Covey C, Dease CG, Doutriaux CM, Drach RS, Fiorino M, Gleckler PJ, Hnilo JJ, Marlais SM, Phillips TJ, Potter GL, Santer BD, Sperber KR, Taylor KE, Williams DN (1999) An overview of the results of the Atmospheric Model Intercomparison Project (AMIP). *Bull Am Meteorol Soc* 80: 29–56
- Gill AE (1982) *Atmosphere–ocean dynamics*, Academic Press, 662 pp.
- Held IM, Hou AY (1980) Nonlinear axially symmetric circulations in a nearly inviscid atmosphere, *J Atmos Sci* 37: 515–533
- Hide R, Dickey JO, Marcus SL, Rosen RD, Salstein DA (1997) Atmospheric angular momentum fluctuations during 1979–1988 simulated by global circulation models, *J Geophys Res* 102: 16423–16438
- Hoerling MP, Ting M, Kumar A (1995) Zonal flow–stationary wave relationship during El Nino: implications for seasonal forecasting, *J Climate* 8: 1838–1852
- Huang HP, Sardeshmukh PD, Weickmann KM (1999) The balance of global angular momentum in a long-term atmospheric data set, *J Geophys Res* 104: 2031–2040
- Huang HP, Weickmann KM, Hsu CJ (2001) Trend in atmospheric angular momentum in a transient climate change simulation with greenhouse gas and aerosol forcing, *J Climate* 14: 1525–1534
- Huang HP, Weickmann KM, Rosen RD (2003) Unusual behavior in atmospheric angular momentum during the 1965 and 1972 El Nino, *J Climate* 16: 2526–2539
- Kalnay E, Kanamitsu M, Kistler R, Collins W, Deaven D, Gandin L, Iredell M, Saha S, White G, Woollen J, Zhu Y, Chelliah M, Ebisuzaki W, Higgins W, Janowiak J,

- Mo KC, Ropelewski C, Wang J, Leetma A, Reynolds R, Jenne R, Joseph D (1996) The NCEP/NCAR 40-year reanalysis project, *Bull Amer Meteor Soc* 77: 437–471
- Kang IS, Lau KM (1994) Principal modes of atmospheric circulation anomalies associated with global angular momentum fluctuations, *J Atmos Sci* 51: 1194–1205
- Karoly DJ, Braganza K (2001) Identifying global climate change using simple indices, *Geophys Res Lett* 28: 2205–2208
- Lambert SJ, Boer GJ (2001) CMIP1 evaluation and intercomparison of coupled climate models, *Clim Dyn* 17: 83–106
- Lindzen RS, Hou AY (1988) Hadley circulations for zonally averaged heating centered off the equator, *J Atmos Sci*, 45: 2416–2427
- Lindzen RS, Nigam S (1987) On the role of sea surface temperature gradients in forcing low-level winds and convergence in the tropics, *J Atmos Sci* 44: 2440–2458
- Madden RA (1987) Relationship between changes in the length of day and the 40- to 50-day oscillation in the Tropics, *J Geophys Res* 92: 8391–8399
- Madden RA, Speth P (1995) Estimates of atmospheric angular momentum, friction, and mountain torques during 1987–1988, *J Atmos Sci* 52: 3681–3694
- Newman M, Compo GP, Alexander MA (2003) ENSO-forced variability of the Pacific decadal variability, *J Climate* 16: 3853–3857
- Oort AH, Yienger JJ (1996) Observed interannual variability in the Hadley circulation and its connection to ENSO, *J Climate* 9: 2751–2767
- Peixoto JP, Oort AH (1992) *Physics of Climate*, American Institute of Physics, New York, 520 pp.

- Räisänen J (2003) CO₂-induced changes in atmospheric angular momentum in CMIP2 experiments, *J Climate* 16: 132–143
- Rosen RD, Eubanks TM, Dickey JO, Steppe JA (1984) An El Nino signal in atmospheric angular momentum and earth rotation, *Science* 225: 411–414
- Santer BD, Wigley TML, Doutriaux C, Boyle JS, Hansen JE, Jones PD, Meehl GA, Roeckner E, Sengupta S, Taylor KE (2001) Accounting for the effects of volcanoes and ENSO in comparisons of modeled and observed temperature trends, *J Geophys Res* 106: 28033–28059
- Seager R, Harnik N, Kushnir Y, Robinson W, Miller J (2003) Mechanisms of hemispherically symmetric climate variability, *J Climate* 16: 2960–2978
- Smith TM, Reynolds RW, Livezey RE, Stokes DC (1996) Reconstruction of historical sea surface temperatures using empirical orthogonal functions, *J Climate* 9: 1403–1420
- Sobel AH, Held IM, Bretherton CS (2002) The ENSO signal in tropical tropospheric temperature, *J Climate* 15: 2702–2706
- Soden BJ (2000) The sensitivity of the tropical hydrological cycle to ENSO, *J Climate* 13: 538–549
- Trenberth KE (1990) Recent observed interdecadal climate changes in the Northern Hemisphere, *Bull Am Meteorol Soc* 71: 988–993
- Yulaeva E, Wallace JM (1994) The signature of ENSO in global temperature and precipitation fields derived from the microwave sounding unit, *J Climate* 7: 1719–1736
- Wallace JM, Hobbs PV (1977) *Atmospheric science, an introductory survey*, Academic

Press, 467 pp.

Weickmann KM, Kiladis GN, Sardeshmukh PD (1997) The dynamics of intraseasonal atmospheric angular momentum oscillations, *J Atmos Sci* 54: 1445–1461

Weickmann KM, Robinson WA, Penland C (2000) Stochastic and oscillatory forcing of global atmospheric angular momentum, *J Geophys Res* 105: 15543–15557

Zhang Y, Wallace JM, Battisti DS (1997) ENSO-like interdecadal variability, *J Climate* 10: 1004–1020

Figure captions

Fig. 1 (a) Observed monthly anomalies of global relative atmospheric angular momentum (AAM) (black) and NINO3.4 SST index (red). Units are AMU ($1 \text{ AMU} = 10^{25} \text{ kg m}^2 \text{ s}^{-1}$) for angular momentum, $^{\circ}\text{C}$ for SST. (b) Same as (a), but the angular momentum is simulated by an AGCM (detailed in Sec. 3) forced by the SST. (c) The 5-yr running means of ΔAAM and ΔSST constructed from the 3-member ensemble mean of a set of global warming simulations using a coupled GCM. The anomaly in this case is defined as the departure from a base value obtained from the average of the first 20 yrs of the runs. See Huang et al. (2001) for background. The arrangement and units for (c) are similar to (a) and (b), except that the ΔSST shown is multiplied by a factor of 0.75.

Fig. 2 The standard deviation of the monthly anomalies of SST on the equator over the Pacific basin for the CMIP2+ models. Observed counterpart from extended Reynolds SST dataset is shown in bold black. A red bar at the bottom indicates the longitudinal extent of the NINO3.4 region.

Fig. 3 Time series of monthly ΔAAM and $\Delta\text{SST}(\text{NINO3.4})$ for an arbitrarily chose 50-yr segment from each coupled model. Black and red are ΔAAM and ΔSST . The arrangement and units are the same as Fig. 1.

Fig. 4 Scatter plots of 9-month low-pass filtered ΔAAM vs. $\Delta\text{SST}(\text{NINO3.4})$ for three selected models. (a) MRI, (b) HadCM3, (c) ECHO. Units are AMU for ΔAAM and $^{\circ}\text{C}$ for ΔSST . A straight line is drawn to indicate the slope, $S_1 = \Delta\text{AAM}/\Delta\text{SST}$, obtained from linear regression.

Fig. 5 The open circles and accompanying vertical sticks are the means and twice the

standard deviations of S_1 obtained from linear regression for the coupled models. The filled circle is the ensemble mean of S_1 calculated from 16 AGCM runs forced by observed SST (see text). The vertical bar associated with the filled circle indicates twice the intra-ensemble standard deviation. The S_1 is defined as $\Delta AAM/\Delta SST$, where ΔSST is the NINO3.4 SST index. Unit of S_1 is AMU/ °C

Fig. 6 Same as Fig. 5, except that S_1 is defined as $\Delta AAM/\Delta SST$ with the ΔSST being a pan-Pacific SST index (see text) averaged over the box bounded by 5°N, 5°S, 150°E, and 90°W.

Fig. 7 Saturation mixing ratio (w_s) over sea surface as a function of SST. Filled circles are exact values; dashed line their linear least square fit for $18^\circ\text{C} < \text{SST} < 32^\circ\text{C}$. Units are g/kg for mixing ratio, °C for SST.

Table 1 The names and developers of the participating CMIP2+ models considered in this study. The long-term mean, standard deviation of monthly anomaly, and standard deviation of 9-month low-pass filtered monthly anomaly of global relative AAM simulated by the models are listed in column 4, 5, and 6 (unit of angular momentum is AMU). The observed counterparts are listed at bottom.

<i>Abbreviation in this paper</i>	<i>Full name of model, developer</i>	<i>Length of run (yr)</i>	<i>Long-term mean, M_R</i>	<i>Monthly std ΔM_R</i>	<i>Monthly std, ΔM_R 9-mon LP</i>
CCCMA	CCCma_CGCM2 Canadian Centre for Climate Modelling and Analysis	80	14.3	0.55	0.38
CSIRO	CSIRO_Mk2 Commonwealth Scientific & Industrial Research Organisation, Australia	100	14.4	0.56	0.33
CSM	CSM1 National Center for Atmospheric Research (NCAR)-led consortium	300	17.9	0.68	0.45
ECHAM	ECHAM4/OPYC3 Max Planck Institute, Germany	150	18.7	0.91	0.62
ECHO	ECHO-G M&D Group, Max Planck Institute, Germany	100	18.6	1.12	0.84
GFDL	GFDL_R30_c NOAA Geophysical Fluid Dynamics Laboratory	300	15.3	0.79	0.56
HADCM2	HadCM2 U.K. Met Office	80	15.7	1.27	1.10
HADCM3	HadCM3 U.K. Met Office	80	16.9	0.90	0.80
MRI	MRI_CGCM2.3 Meteorological Research Institute, Japan	150	18.0	1.20	1.06
PCM	PCM NCAR & U.S. Department of Energy	300	17.2	0.80	0.60
Observation	(1979–1998)		14.7	1.07	0.90

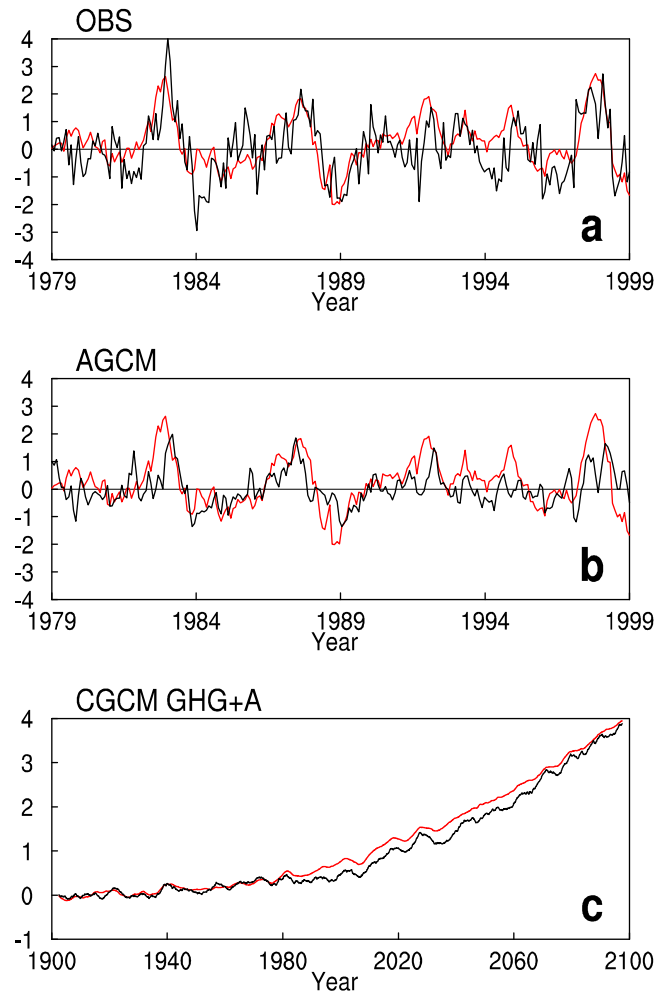


Fig. 1

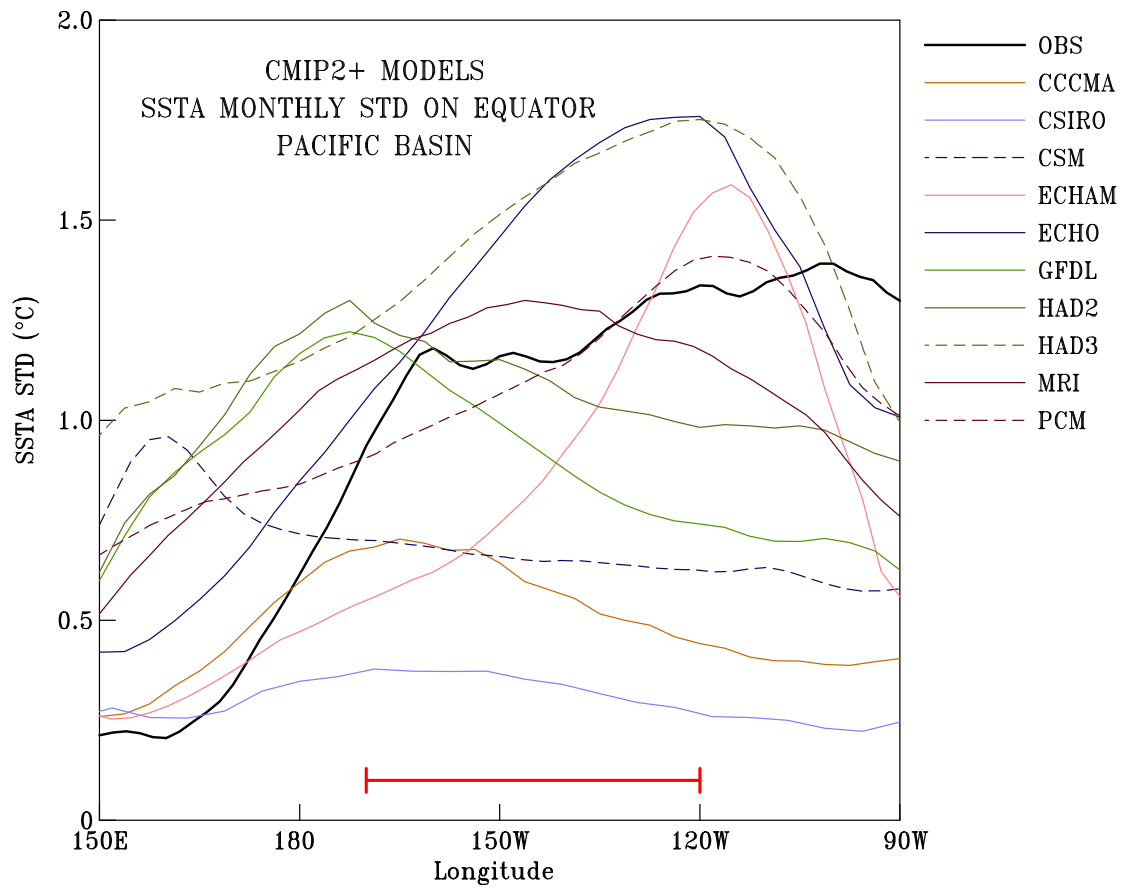


Fig. 2

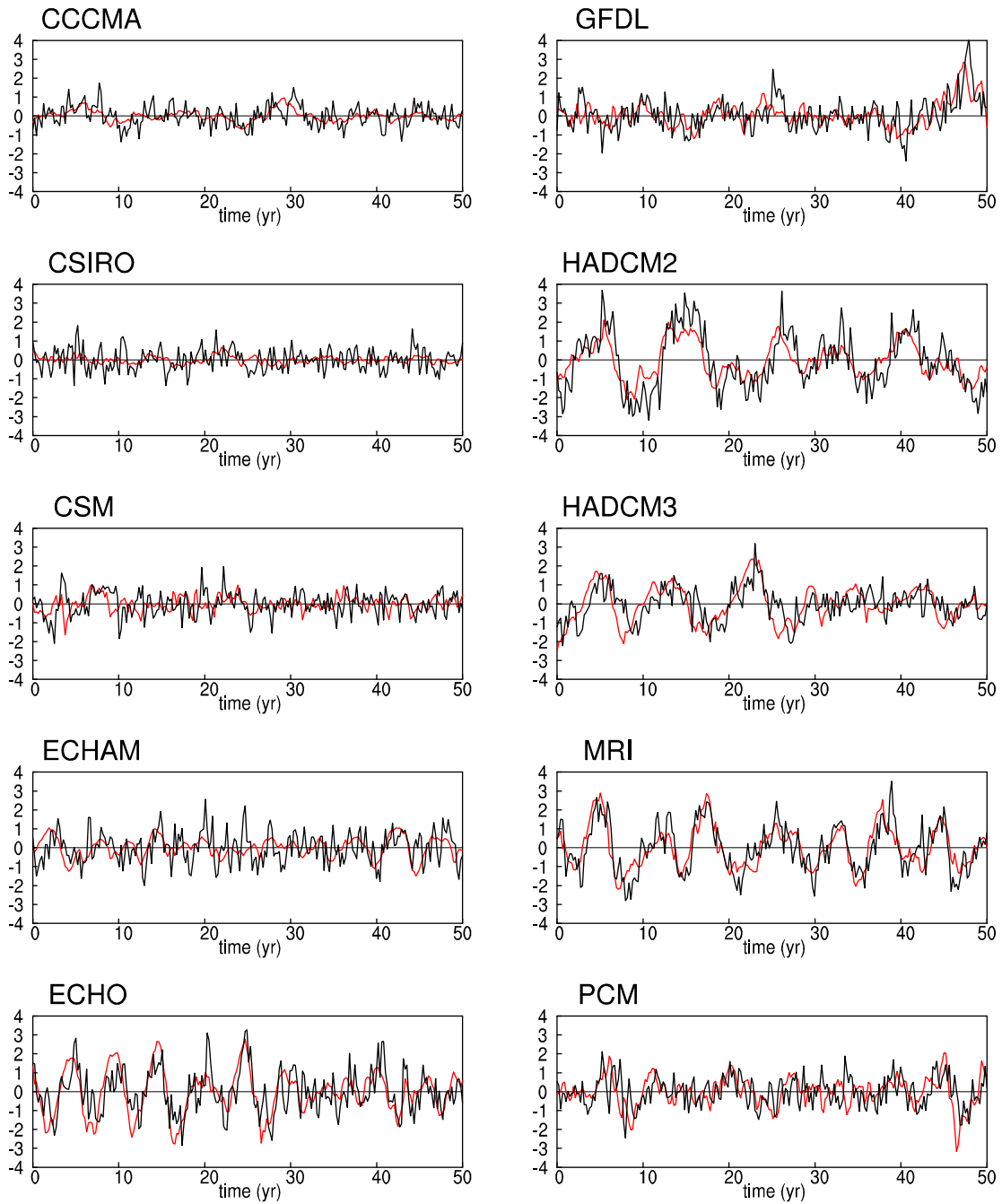


Fig. 3

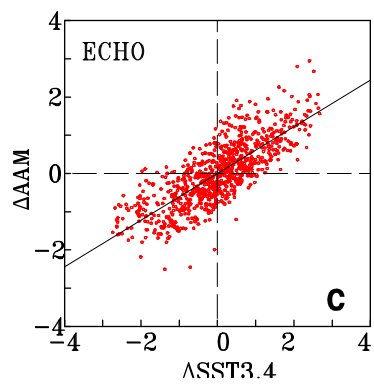
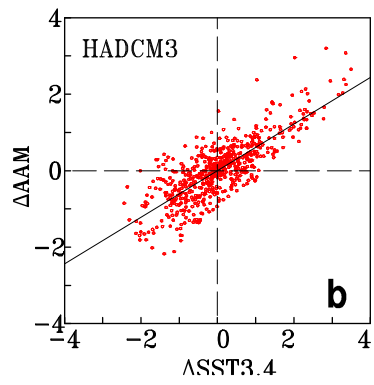
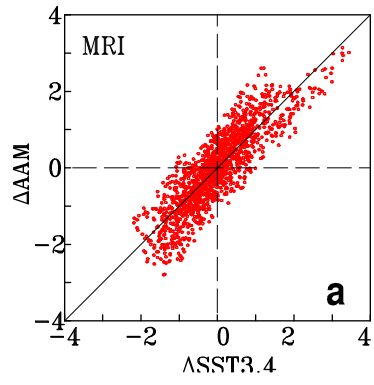


Fig. 4

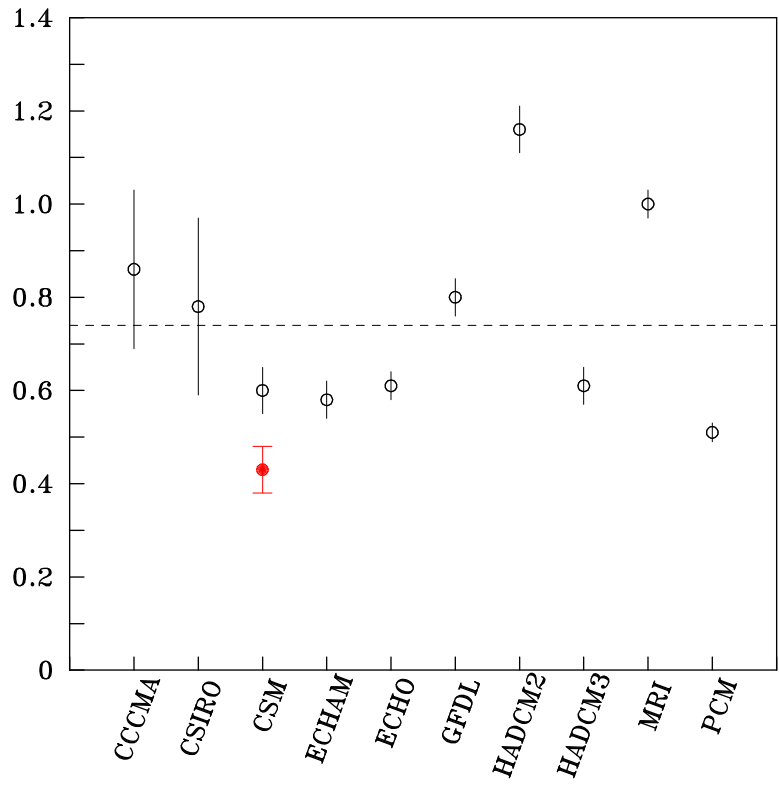


Fig. 5

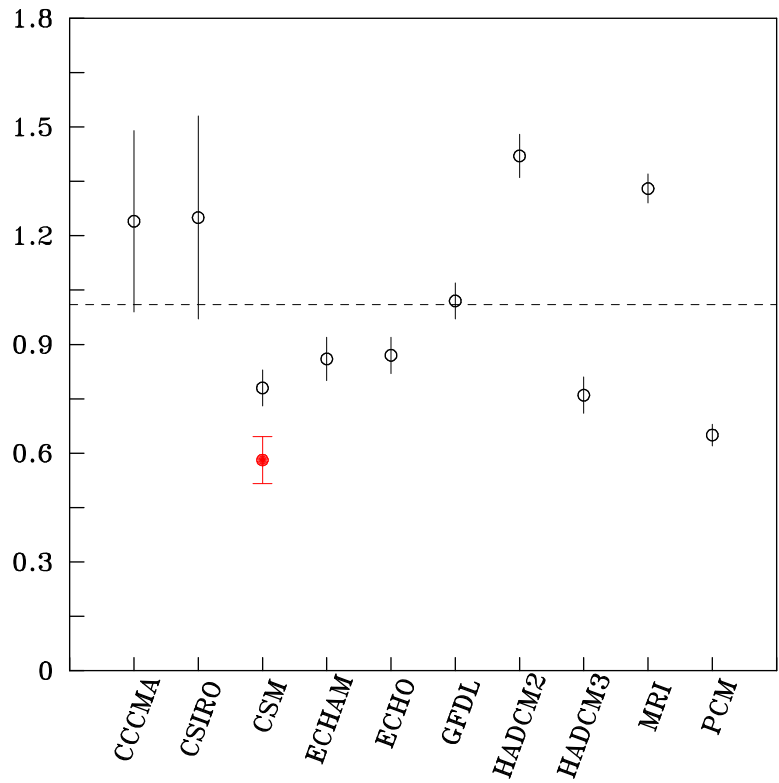


Fig. 6

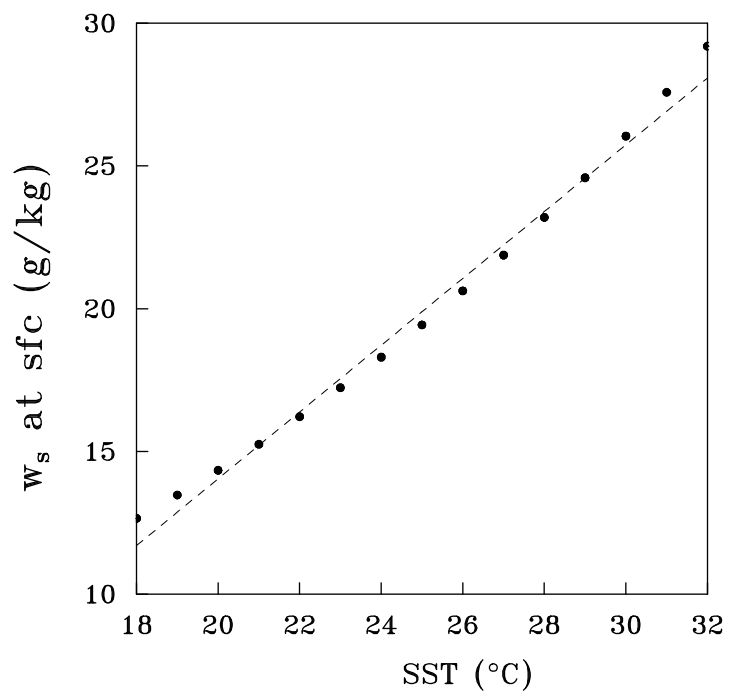


Fig. 7